Influence of plasma triangularity and collisionality on electron heat transport in ECH dominated TCV L-mode plasmas

Y Camenen[1], A Pochelon[1], A. Bottino[1], S. Coda[1], F. Ryter[2], O. Sauter[1], R. Behn[1], T.P. Goodman[1], M.A. Henderson[1], A. Karpushov[1], L. Porte[1], G. Zhuang[1]

[1] Centre de Recherches en Physique des Plasmas, Association EURATOM-Confédération Suisse, Ecole Polytechnique Fédérale de Lausanne (EPFL), CH-1015 Lausanne, Switzerland

[2] Max-Planck-Institut für Plasmaphysik, EURATOM-IPP Association, Garching, Germany

E-mail: yann.camenen@epfl.ch

Abstract.

Submitted to: *Plasma Phys. Control. Fusion*

1. Introduction

Improving the energy confinement is a way to increase the plasma temperature towards the conditions required for plasma ignition, keeping constant the input power. As the energy confinement of tokamak plasmas is degraded by cross-field electron heat transport, the energy confinement improvement is linked to a better understanding of electron transport. A fraction of cross-field transport arises from Coulomb collisions and is described, in toroidal geometry, by the neoclassical theory. The remaining part, one or two orders of magnitude higher, is attributed to micro-turbulence, an active field of investigation where large progress has been achieved in the recent years, in particular in the simulation of plasma micro-instabilities. The experimental findings of electron heat transport dependence on controlled plasma parameters is of use for improving plasma performance and providing an easier access to low transport regimes like the electron internal transport barrier (eITB) regime, but equally for predicting energy confinement in future fusion devices, by providing experimental data to test the relevance of micro-instabilities simulations and/or to establish heuristic transport models.

The present study explores the experimental dependence of electron heat transport on electron temperature, electron temperature gradient, plasma shape and plasma collisionality in TCV. The electron temperature and electron temperature gradient

are predicted to have a strong influence on the trapped electron (TE) and electron temperature gradient (ETG) modes growth rate and have been shown experimentally to strongly modify the level of electron transport [ASDEX JET TORE SUPRA...]. Plasma shape is one of the fundamental parameters in a tokamak that strongly influences plasma properties and performance, placing also strong constraints on technological and construction choices in machine design. Increasing the elongation allows higher plasma current and also influences other operational limits such as the pressure [1, 2] and density limits [3]. Triangularity and elongation have a strong influence on the core stability, e.g. sawtooth stability [4], and on edge plasma, in particular on H-mode pedestal and ELM stability [5, 6]. Global confinement studies in Ohmic [7, 8, 9] and in central EC heated L-mode plasmas [10, 11] showed the beneficial role of low or negative triangularity on the electron energy confinement time. On the contrary, similar studies in H-mode showed that, due to the contribution of the edge pedestal, the confinement time increases with plasma triangularity [5, 6]. For the study of electron heat transport, L-mode plasmas seems to be good candidates to minimizes the influence of the plasma edge on global confinement, allowing a more direct study of the genuine effect of plasma shape. Concerning plasma collisionality, it has been shown recently to play an essential role in particle transport [12, 13]. At low collisionality, central EC heating leads to a flattening of the density profile, whereas at high collisionality it leads to a peaking of the density profile [14]. This behavior has been attributed to a change of the dominant micro-instability, from TE mode at low collisionality to ITG mode at high collisionality [12]. The stabilization of TE mode at high plasma collisionality is also expected to influence electron heat transport.

The specificity of the present study lies in the exploration of a large range of both electron temperature gradients and electron temperatures, allowing to decouple the effect of these two quantities, but also in the investigation of the influence of plasma shaping, in particular the plasma triangularity, which is varied from negative to positive values, $-0.4 < \delta < 0.4$.

2. Electron temperature, electron temperature gradient and plasma triangularity variation

2.1. TCV description

The TCV tokamak (major radius $R_0 = 0.88\,\mathrm{m}$, minor radius $a < 0.255\,\mathrm{m}$, magnetic field $B_\mathrm{T} < 1.54\,\mathrm{T}$, plasma current $I_\mathrm{p} < 1\,\mathrm{MA}$) is designed to investigate the effects of plasma cross-section shaping. Plasma edge triangularity $-0.7 < \delta < 1$ and plasma edge elongation $0.9 < \kappa < 2.8$ have been achieved [9]. The auxiliary heating relies on electron cyclotron (EC) waves, usually polarized in X-mode, at the 2^{nd} harmonic (X2) and at the 3^{rd} harmonic (X3) frequencies, allowing the coupling of the power to any plasma shape. The X2 EC waves are produced at 82.7 GHZ by six gyrotrons delivering a total nominal power of 3 MW and are coupled to the plasma from the low field side,

using six independent launchers steerable during the discharge [15]. The X3 EC waves are produced at 118 GHz by three gyrotrons delivering a total nominal power of 1.5 MW and are coupled to the plasma from the top, using a single launcher that can also be steered during the discharge [16].

2.2. Plasma discharges and experimental conditions

Two sets of experiments have been performed to study the electron heat transport of L-mode plasmas in limiter configuration.

The "constant I_p" set of experiments is dedicated to the study of the dependence of electron heat transport on the electron temperature T_e and on the normalized electron temperature gradient $R/L_{T_\mathrm{e}} = R\nabla T_\mathrm{e}/T_\mathrm{e}$. The toroidal magnetic field B_T, the plasma elongation κ and the plasma current I_p are kept constant ($B_\mathrm{T} = 1.44\,\mathrm{T}$, $\kappa = 1.6$ and $I_\mathrm{p} = 220\,\mathrm{kA}$), while two plasma triangularities are achieved, $\delta = 0.2$ and $\delta = 0.4$, with an edge safety factor q_{95} close to 5 (4.7 and 5.4, respectively). The temperature profile is modified by depositing 0.45 to 1.8 MW of radially localized X2 EC heating power at two different radial locations: one off-axis at $\rho_1 = 0.35$, just outside the $q = 1$ surface, and one far off-axis at $\rho_2 = 0.7$. Here, we define the normalized radius as $\rho = \sqrt{V/V_\mathrm{LCFS}}$, where V and V_LCFS are the volumes delimited by the flux surface labelled by ρ and by the last closed flux surface, respectively. The sawtooth period response to the EC heating confirms that the EC power deposition at ρ_1 occurs just outside the $q = 1$ surface, as indicated by the increase of the sawtooth period (sawtooth stabilization) while increasing the power deposited at ρ_1, from $2-3\,\mathrm{ms}$ in Ohmic to above 10 ms with the total EC power. [17].

The "constant q_{95}" set of experiments focuses on the role of the plasma triangularity and special care is taken to achieve the same line averaged density, total power and EC power deposition radius in each plasma configuration. The toroidal magnetic field and the plasma elongation are kept constant ($B_\mathrm{T} = 1.44\,\mathrm{T}$, $\kappa = 1.5$, but the plasma current is changed so as to keep the edge safety factor constant, $q_{95} = 3.5$, while a large range of plasma triangularity, from negative to positive values, is explored ($-0.4 < \delta < +0.4$).

In both the "constant I_p" and "constant q_{95}" sets, the density range is fixed to $0.8 < \overline{n}_\mathrm{e} < 1.8 \cdot 10^{19}\,\mathrm{m}^{-3}$, such as to avoid excessive refraction of the EC beams ($n_\mathrm{eo}/n_{\mathrm{e\,cut-off}} < 0.7$) and to ensure full single pass absorption for the far off-axis deposition. The width of the EC beams, narrow compared to the plasma height, allows for radially localized EC power deposition. The EC power deposition width at half height $\Delta\rho_\mathrm{EC}$ does not exceed 0.1 and the power absorption is above 95%, as computed by the linear ray tracing code TORAY-GA [18]. A poloidal view of the plasma cross-section and of the EC beams is shown in figure 1, for simultaneous central and off-axis EC power deposition in a plasma with a triangularity $\delta = 0.4$.

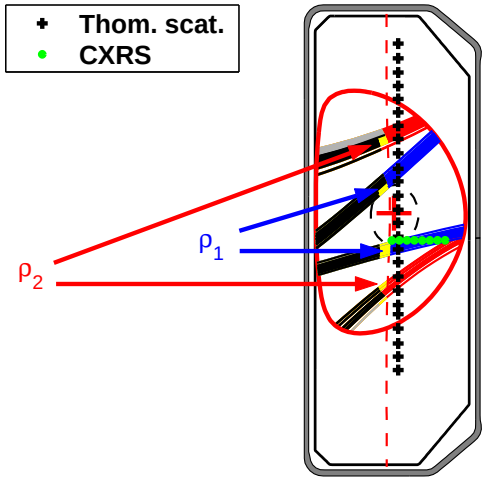

Figure 1. Poloidal view of the plasma cross section, $\delta = 0.4$ and $\kappa = 1.6$, and of the EC beams for simultaneous EC power deposition at ρ_1 and ρ_2. The cold resonance is indicated by the dashed line and the q=1 surface by the dashed circle. The Thomson scattering and CXRS measurements location are indicated by crosses and dots, respectively.

2.3. Electron temperature profile and discharge response

The measurement of the electron density n_e and electron temperature T_e profiles, essential for this study, relies on Thomson scattering yielding coverage of the full plasma height with a spatial resolution of 4.5 cm, typically 2×8 points in a profile, as shown in figure 1. The profiles are measured every 25 ms and averaged over ~ 300 ms after stationary internal inductance l_i is reached. The normalized temperature and density gradients, R/L_{T_e} and R/L_{n_e}, are calculated by mapping the temperature and density profiles on a real spatial coordinate chosen as the distance, measured at the outer mid-plane, from the torus axis to the considered flux surface.

Changing the amount of EC power deposited in the plasma and its spatial distribution allows to change the electron temperature profile. Increasing the amount of EC power deposited at ρ_1 only, from 0.45 to 1.8 MW, allows increasing T_e without changing significantly the normalized temperature gradient: R/L_{T_e} only varies by 10% in the confinement region. This behavior, already observed in several tokamaks, is called profile stiffness [19]. In order to change the value of R/L_{T_e}, far off-axis distribution of part or totality of the EC power launched is needed, following the scheme developed in ASDEX Upgrade to study electron heat transport as a function of the normalized electron temperature gradient [20]. Far off-axis EC power deposition at ρ_2 leads to low R/L_{T_e} values in the region of investigation, $\rho_1 < \rho < \rho_2$, whereas off-axis deposition at ρ_1 leads to high R/L_{T_e} values. Intermediate R/L_{T_e} values are achieved by sharing the deposited EC power off-axis and far off-axis. In the "constant I_p" set of experiments, the variation of the total EC power and of the EC power distribution has allowed the achievement of strong variations of both T_e and R/L_{T_e} at mid-radius. The variation

of these two parameters at $\rho = 0.53$ is shown in figure 2, together with data from ASDEX Upgrade for similar experiments. ASDEX Upgrade experiments are achieved in L-mode plasmas in divertor configuration, with a plasma elongation $\kappa = 1.6$ and a plasma triangularity $\delta = 0.25$. The edge safety factor $q_{95} = 4.5$ and the total EC power $P_{EC} = 1.3\,\mathrm{MW}$ are kept constant [19].

The flux surface averaged gradient of ρ, $< |\nabla\rho| >$, does not vary significantly with

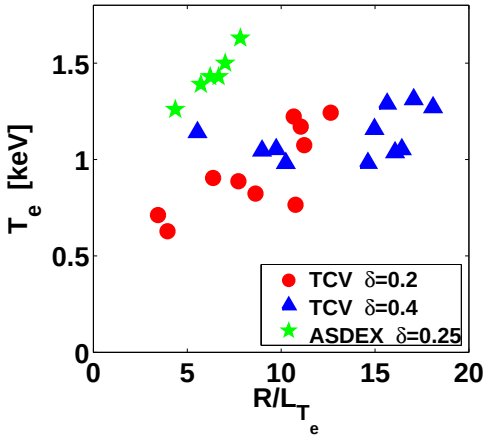

Figure 2. Range of electron temperature T_e and normalized temperature gradient R/L_{T_e} explored at $\rho = 0.53$ in TCV and in similar ASDEX Upgrade electron heat transport experiments.

plasma triangularity (less than 5% at mid-radius). The higher R/L_{T_e} values obtained at $\delta = 0.2$ as compared to $\delta = 0.4$ are therefore not an artifact of the geometry due to the mapping of the T_e profile on a real space coordinate.

The relation between the electron temperature T_e and the electron heat flux Q_e, an indication of the level of cross-field electron heat transport, is obtained by calculating the electron thermal diffusivity χ_e defined by

$$Q_\mathrm{e} = -n_\mathrm{e}\chi_\mathrm{e} < |\nabla\rho|^2 > \frac{\partial T_\mathrm{e}}{\partial\rho}$$

where the brackets indicate an average over the flux surface. As a linear relation between the electron heat flux Q_e and the electron temperature gradient ∇T_e is assumed, the effect of off-diagonal terms in the transport matrix is not included. The electron heat flux is computed in steady-state taking into account the contributions of the Ohmic power, the EC power, and the power transferred from the electrons to the ions. A radially uniform loop voltage is assumed for the calculation of the Ohmic power, and the EC power deposition is obtained from the TORAY-GA ray tracing code. The ion temperature profile, needed to estimate the power transfer to the ions, is obtained from the Charge Exchange Recombination Spectroscopy diagnostic viewing the plasma region indicated in figure 1. The low plasma density results in a low equipartition power flow from the electrons to the ions and a high $T_\mathrm{e}/T_\mathrm{i}$ ratio. The radiated power

$P_{\rm rad}$ measured by XUV-bolometer photodiodes never exceeds 20% of the total power $P_{\rm tot}$. Moreover, the ratio $P_{\rm rad}/P_{\rm tot}$ remains below 5% for $\rho < 0.8$ and the radiated power is therefore negligible in the region of investigation $\rho_1 < \rho < \rho_2$. As shown in

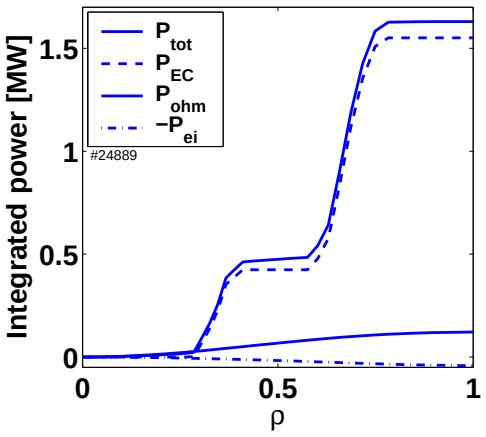

Figure 3. Power balance analysis showing the contributions of the EC power $P_{\rm EC}$, the Ohmic power $P_{\rm ohm}$ and the equipartition power $P_{\rm ei}$ to the total power $P_{\rm tot}$, for a case at $\delta = 0.4$ with 0.45 MW of EC power deposited at ρ_1 and 1.35 MW deposited at ρ_2.

figure 3, the power balance is strongly dominated by the EC power. A change in the radial EC power distribution allows for a large variation of $Q_{\rm e}$ between ρ_1 and ρ_2 while keeping constant $Q_{\rm e}^{\rm edge}$. In the following, the local quantities are given at a normalized radius of $\rho = 0.53$, sufficiently far from the two EC power deposition radii, ρ_1 and ρ_2, to avoid large uncertainties on $Q_{\rm e}$ which could arise from the radial uncertainty of the EC power deposition calculations.

In the "constant $I_{\rm p}$" set of experiments, the EC waves are launched in the poloidal plane to achieve pure heating. The current drive component, due to the small angle with the magnetic field, represents less than 2% of the total plasma current, as evaluated using TORAY-GA. In the "constant q_{95}" set of experiments, a small toroidal angle was added to the EC waves to compensate for the inclination of the magnetic field lines and to reduce to zero the current drive component. The plasma current density profile is calculated using the transport code PRETOR [] in interpretative mode, consistently taking into account the experimental pressure profiles and the current density sources, Ohmic and bootstrap (EC driven current negligible), to reconstruct the magnetic equilibrium assuming steady-state conditions.

The neoclassical plasma resistivity depends on the plasma effective charge $Z_{\rm eff}$, which is estimated from the experimental temperature and density profiles, loop voltage and plasma current, assuming a flat $Z_{\rm eff}$ profile. The $Z_{\rm eff}$ value is estimated so as to match the value of the calculated total plasma current, taking into account the Ohmic and bootstrap contributions, with the value of the experimental one.

3. Micro-instabilities simulation

Let us first investigate the stability of electron temperature gradient (ETG), trapped electron (TE) and ion temperature gradient (ITG) modes, which are potentially responsible for anomalous heat transport in these experiments. The temperature gradient threshold of the ETG instability derived from linear gyro-kinetic simulations [21] is found to be at least two times higher than the experimental values of R/L_{T_e} in the region $0.2 < \rho < 0.7$, due to the high Z_eff and $T_\mathrm{e}/T_\mathrm{i}$ values. The ETG modes are therefore predicted to be stable in the region of investigation. On the other hand, local gyro-fluid linear simulations using GLF23 [22] indicate that TE and ITG modes are unstable. The experimental values of the TE mode driving terms, R/L_{T_e} and R/L_{n_e}, at $\rho = 0.53$, are shown in figure 4. For most of the experimental conditions, the dominant instability

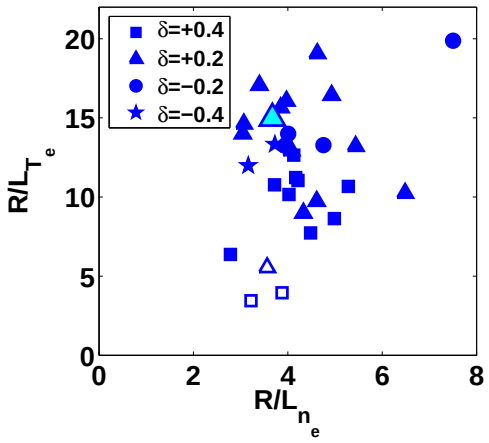

Figure 4. Experimental values of the driving gradients for TE modes, R/L_{T_e} and R/L_{n_e} at $\rho = 0.53$. From GLF23 simulations, the dominant instability exhibits a TE mode behavior (full symbols), except for the lowest values of R/L_{T_e} (open symbols). The big symbol indicates a point also evaluated in LORB5 simulations.

exhibits a TE mode behavior (full symbols in figure 4). First, in the simulations, the linear mode growth rate γ decreases strongly when R/L_{T_e} is reduced and increases when R/L_{T_i} is reduced. Secondly, γ is insensitive to $T_\mathrm{e}/T_\mathrm{i}$ when T_e is kept constant, whereas γ strongly increases with $T_\mathrm{e}/T_\mathrm{i}$ when T_i is kept constant. For the lowest R/L_{T_e} values, the dominant instability exhibits an ITG mode behavior (empty symbols in figure 4). In particular, γ increases strongly with R/L_{T_i} and is nearly insensitive to R/L_{T_e}.
However, in all the cases of figure 4, the mode frequency ω_r is in the same direction than the ion drift frequency ω_Di, which is the characteristic of an ITG mode. It could suggest that even if the dominant instability is an ITG mode, the TE mode is also strongly unstable, and the ITG mode growth rate is affected by the coupling between ITG and TE modes. Another possibility is that the GLF23 '8 equations' version without impurity dynamics, used in our simulation, is no longer valid to predict ω_r at high Z_eff values ($Z_\mathrm{eff} = 2.5{-}5$ in the present experiments).
Global collisionless gyro-kinetic simulations have been performed with the linear code

LORB5 [23] for the point indicated in figure 4. The mode growth rate $\gamma = \gamma_{\mathrm{p,i}} + \gamma_{\mathrm{d,i}} + \gamma_{\mathrm{d,e}}$ is calculated for toroidal mode numbers n ranging from 10 to 25. The quantities $\gamma_{\mathrm{p,i}}$, $\gamma_{\mathrm{d,i}}$ and $\gamma_{\mathrm{d,e}}$ indicate respectively the contribution of the ion parallel velocity, the ion drift velocity and the electron drift velocity terms to the total mode growth rate. The contribution of the electronic channel is found to be more than 90% for all toroidal mode numbers (maximum growth rate obtained for $n = 25$). The mode frequency indicates a TE mode nature and the electrostatic potential fluctuations are localized between $\rho = 0.4$ and $\rho = 0.8$.

Gyro-fluid and gyro-kinetic simulations show that in these experiments the stability of the TE mode should play a crucial role in the transport of electron heat. For the present experiment, the variation of the relevant parameters for the stability of ITG/TE modes are given in table 1 at the investigation radius location ($\rho_{\mathrm{vol}} = 0.53$). As in [24] we define an effective collisionality $\nu_{\mathrm{eff}} = \nu_{\mathrm{ei}}/\omega_{\mathrm{De}} \approx 0.1R\frac{n_{\mathrm{e}}Z_{\mathrm{eff}}}{T_{\mathrm{e}}^2}$, relevant to study the impact of collisions on electron heat transport (attributed to TE and ITG modes) as it compares the collision frequency ν_{ei} to the electron drift frequency ω_{De}, a rough estimate of the mode growth rate. f_{t} is the trapped particle fraction [25].

Table 1. Range of parameters, relevant for the stability of ITG/TE modes, explored in the present experiments.

T_{e} [keV]	T_{i} [keV]	$T_{\mathrm{e}}/T_{\mathrm{i}}$	$R/L_{T_{\mathrm{e}}}$	$R/L_{T_{\mathrm{i}}}$	$R/L_{n_{\mathrm{e}}}$
0.6-1.3	0.2-0.5	2-4	4-20	3.5-6.5	3-7.5

f_{t}	$n_{\mathrm{e19}}Z_{\mathrm{eff}}$ [$10^{19}\mathrm{m}^{-3}$]	ν_{eff}	q	s
0.54-0.55	3.4-11.5	0.25-1	1.5-1.9	1.1-1.6

4. Experimental heat diffusivity dependence on T_e and $R/L_{T_{\mathrm{e}}}$

4.1. Experimental observations

To investigate the effect of temperature T_{e} and normalized temperature gradient $R/L_{T_{\mathrm{e}}}$ on electron heat transport, we concentrate on the plasma configuration of the "constant I_{p}" set of experiments with triangularity $\delta = 0.4$. The values of T_{e} and $R/L_{T_{\mathrm{e}}}$ are varied over a large range at mid-radius ($T_{\mathrm{e}} = 0.7{-}1.3\,\mathrm{keV}$ and $R/L_{T_{\mathrm{e}}} = 3.4{-}12.6$), while the values of $n_{\mathrm{e}}Z_{\mathrm{eff}}$ and T_{i} remains nearly constant ($n_{\mathrm{e}}Z_{\mathrm{eff}} = 3.5{-}4.5 \times 10^{19}\,\mathrm{m}^{-3}$ and $T_{\mathrm{i}} = 0.20{-}0.25\,\mathrm{keV}$). By changing both the total deposited EC power and the EC power distribution, the correlation between T_{e} and $R/L_{T_{\mathrm{e}}}$ is reduced and a variation of T_{e} by a factor of 1.7 is obtained at constant $R/L_{T_{\mathrm{e}}}$, see figure 2. The heat diffusivity χ_{e}, calculated at $\rho = 0.53$, exhibits a strong dependence on T_{e}, as shown in figure 5, with little scatter despite the large variations of $R/L_{T_{\mathrm{e}}}$ and $R/L_{n_{\mathrm{e}}}$. In comparison, the dependence of χ_{e} on $R/L_{T_{\mathrm{e}}}$ or $R/L_{n_{\mathrm{e}}}$, shown in figure 6, is much weaker and the trend of χ_{e} to increase with $R/L_{T_{\mathrm{e}}}$ can be attributed to the correlation of T_{e} and $R/L_{T_{\mathrm{e}}}$ visible

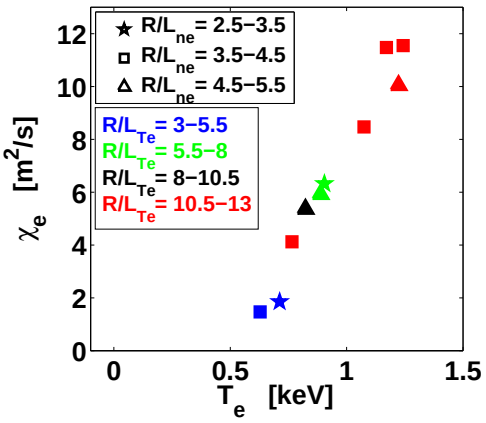

Figure 5. Strong dependence of the experimental electron heat diffusivity χ_e, at mid-radius, on the electron temperature T_e. The ranges of R/L_{n_e} and R/L_{T_e} values are indicated by symbols and colors, respectively.

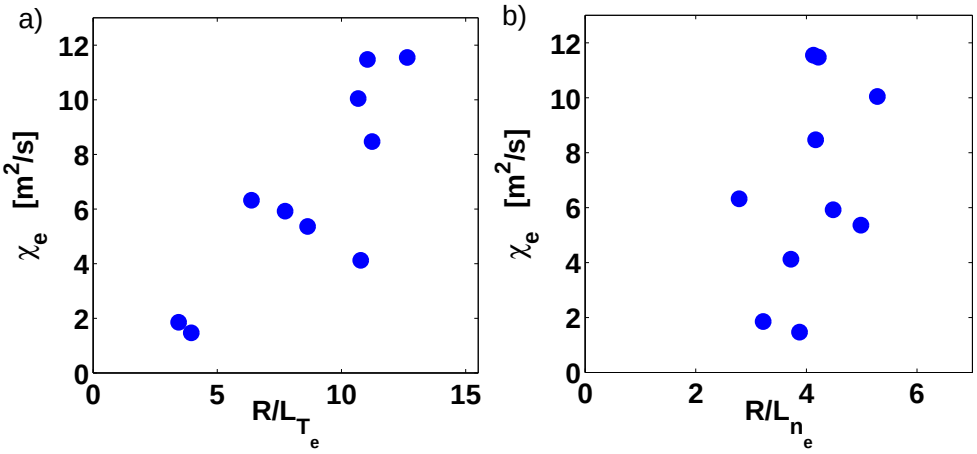

Figure 6. Electron heat diffusivity χ_e, at mid-radius, as a function of (a) R/L_{T_e} and (b) R/L_{n_e}.

in figure 2. The experimental observation of a strong dependence of χ_e on T_e does not exclude a dependence on R/L_{T_e} or R/L_{n_e}, but this dependence has to be rather weak, in contrast to the results from GLF23 linear simulations, which indicate a clear and strong χ_e dependence on both R/L_{T_e} and R/L_{n_e}, as shown in figure 7.

Here, we must stress that in the present stationary experiments, the variation of the temperature profile leads to a change of the current profile. The magnetic shear at mid-radius s increases with T_e from 1.1 to 1.55, which is expected to modify the electron heat transport. However, recent experiments in TCV show that χ_e is approximately proportional to s for $s > 0$ [26]. In the present experiments, the contribution of the shear variation to the variation of χ_e would therefore not exceed 5% of the total increase of χ_e.

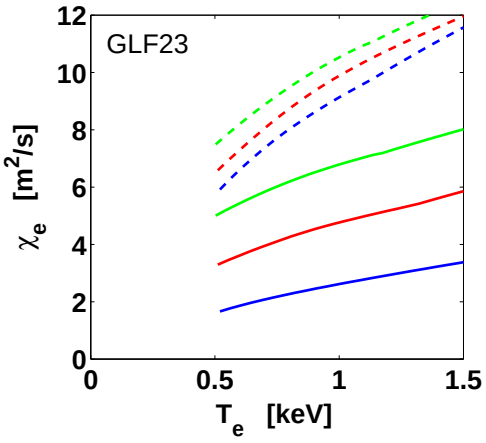

Figure 7. GLF23 simulation of the electron heat diffusivity χ_e, at mid-radius, as a function of T_e, for various R/L_{T_e} and R/L_{n_e} values: $R/L_{T_e} = 6$ (blue), $R/L_{T_e} = 10$ (red), $R/L_{T_e} = 14$ (green), $R/L_{n_e} = 3$ (——), $R/L_{n_e} = 5$ (- - - -). Experimental values (#24890, $\delta = 0.4$) are used and kept constant for the other parameters: $T_i = 0.2\,\mathrm{keV}$, $n_e = 1.25 \times 10^{19}\,\mathrm{m}^{-3}$, $Z_{\mathrm{eff}} = 3$

.

4.2. Gyro-Bohm normalization

An electron heat diffusivity dependence on the electron temperature is predicted by the gyro-Bohm scaling []:

$$\chi_e^{GB} \propto \frac{T_e^{3/2}}{aB^2}$$

where a and B are the plasma minor radius and magnetic field, respectively. We note $f_{GB} = \frac{T_e^{3/2}}{aB^2}$. To test the χ_e dependence on R/L_{T_e}, once the gyro-Bohm scaling is taken into account, we plot χ_e/f_{GB} as a function of R/L_{T_e} in figure **??**a, for the two triangularities of the "constant I_p" set of TCV experiments and for ASDEX Upgrade data. We can first observe, on TCV and ASDEX Upgrade data, that for low values of the normalized temperature gradient, mainly $R/L_{T_e} < 10$, χ_e/f_{GB} increases with R/L_{T_e}, whereas for highest values of R/L_{T_e}, there are no more dependence of χ_e/f_{GB} on R/L_{T_e}. Then, we can note that the gyro-Bohm scaling does not account for the whole dependence of χ_e on T_e: the four points at $\delta = 0.4$ with $R/L_{T_e} \sim 11$ still exhibit significantly different χ_e/f_{GB} values. This is more explicitly shown in figure **??**b where χ_e/f_{GB} still increases with T_e. The different levels of transport observed between TCV plasmas with a triangularity of $\delta = 0.2$ and $\delta = 0.4$ will be addressed in the next sections.

Concerning the heuristic critical gradient model for the heat diffusivity [27, 28], the present data does not allow to state the existence or the non-existence of a threshold in R/L_{T_e} for electron heat transport. However, figure **??**a suggests strongly to include a weaker dependence on R/L_{T_e} in the heuristic gradient model, for high R/L_{T_e} values. For instance, $\chi_e \propto 1 - \frac{R/L_{T_e}^{\mathrm{crit}}}{R/L_{T_e}}$ seems more adequate than $\chi_e \propto R/L_{T_e} - R/L_{T_e}^{\mathrm{crit}}$. Such

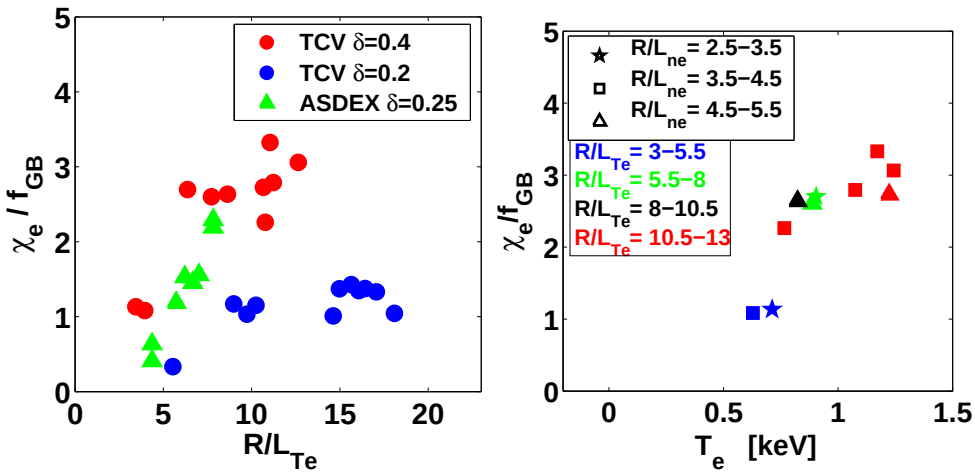

Figure 8. a) Electron heat diffusivity normalized to a gyro-Bohm scaling, as a function of R/L_{T_e}, for TCV and ASDEX Upgrade data
b) Electron heat diffusivity normalized to a gyro-Bohm scaling as a function of T_e, for TCV data at $\delta = 0.4$. The ranges of R/L_{n_e} and R/L_{T_e} values are indicated by symbols and colors, respectively.

a dependence is supported by recent quasi-linear[Peeters 2005] and non-linear [Jenko Dannert 2005] simulations for TE modes.

5. Plasma shape effect

5.1. Experimental results

To investigate the effect of plasma triangularity δ on electron heat transport, we compare two plasmas, from the "constant q_{95}" set of experiments, with negative and positive triangularities, $\delta = -0.4$ and $\delta = +0.4$, keeping constant all controlled plasma parameters in the two plasmas configurations. The line averaged density measured on a central chord of the far infra-red interferometer is maintained constant, $\overline{n}_e = 1.4 \cdot 10^{19}\,\mathrm{m}^{-3}$, as well as the edge safety factor, $q_{95} = 3.5$, and the total deposited EC power, $P_{EC} = 1.3\,\mathrm{MW}$. The edge safety factor is maintained constant by adjusting the total plasma current: $I_p = 265\,\mathrm{kA}$ at $\delta = -0.4$ and $I_p = 295\,\mathrm{kA}$ at $\delta = +0.4$. As the EC power strongly dominates the power balance, the variation of the ohmic power due to the change in plasma current does not change significantly the electron edge heat flux.

A clear reduction of electron heat transport is observed towards negative triangularities. The electron temperature is found to be substantially higher, and the electron heat diffusivity lower, at $\delta = -0.4$ than at $\delta = +0.4$, see figure 9. In the two cases, the electron density and safety factor profiles are similar. The electron heat flux profiles are also similar, except for $\rho < 0.45$ due to a slightly more off-axis EC power deposition at $\delta = -0.4$ as compared to $\delta = -0.4$. The ion temperature follows the same trend than

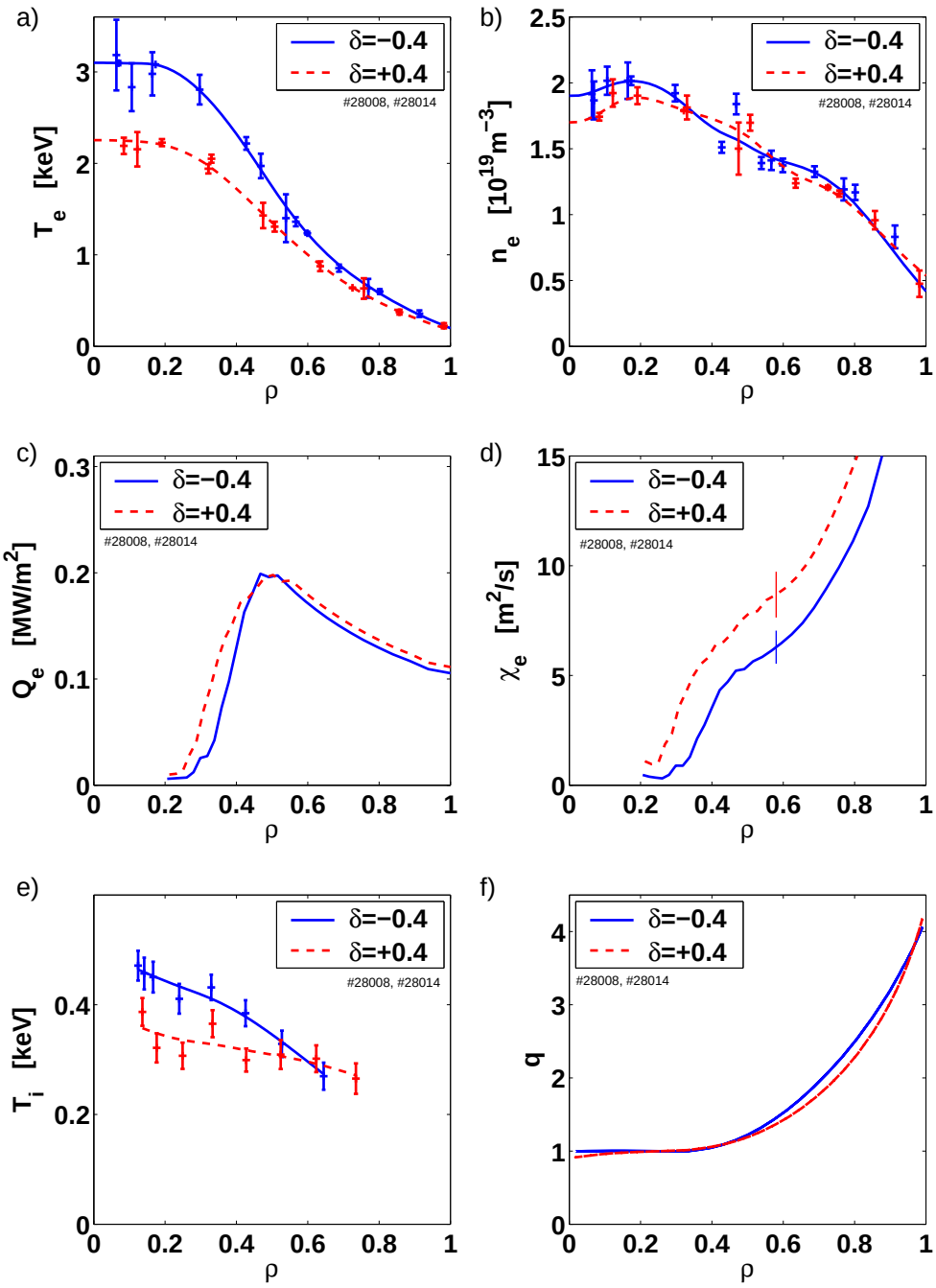

Figure 9. Electron temperature (a) increase obtained by reducing the plasma triangularity from $\delta = -0.4$ (——) to $\delta = +0.4$ (– – –), keeping the electron density (b), the edge safety factor and the electron heat flux (c) constant. The electron heat diffusivity (d) reduces with the plasma triangularity (error bars indicated at $\rho = 0.58$). The ion temperature (e) is increased by the plasma triangularity reduction, while the safety factor profile (f) remains similar.

the electron temperature and is higher at $\delta = -0.4$ than at $\delta = +0.4$. To evaluate the impact of the small variations of Q_e, n_e, and $< |\nabla\rho|^2 >$ in the variation of χ_e with δ,

we calculate:

- Profile 1: χ_e at $\delta = -0.4$
- Profile 2: χ_e using as inputs the values of Q_e, n_e, $< |\nabla\rho|^2 >$ at $\delta = +0.4$ and the value of $\frac{\partial T_e}{\partial \rho}$ at $\delta = -0.4$
- Profile 3: χ_e using as inputs the values of Q_e, n_e, $< |\nabla\rho|^2 >$ at $\delta = -0.4$ and the value of $\frac{\partial T_e}{\partial \rho}$ at $\delta = +0.4$
- Profile 4: χ_e at $\delta = +0.4$

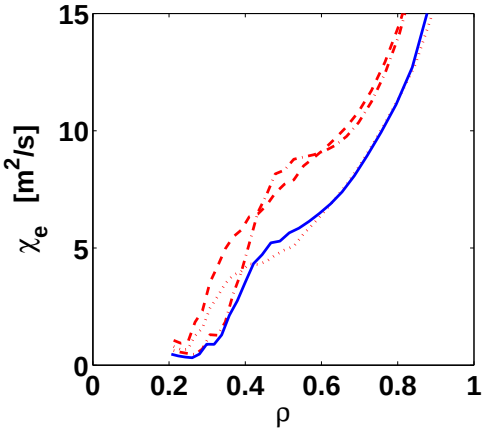

Figure 10. Power balance electron heat diffusivity profile:
1: (——) calculated at $\delta = -0.4$
2: (· · · · · ·) calculated with the values of Q_e, n_e, $< |\nabla\rho|^2 >$ at $\delta = +0.4$ and the value of $\frac{\partial T_e}{\partial \rho}$ at $\delta = -0.4$
3: (— · —) calculated with the values of Q_e, n_e, $< |\nabla\rho|^2 >$ at $\delta = -0.4$ and the value of $\frac{\partial T_e}{\partial \rho}$ at $\delta = +0.4$
4: (- - - -) calculated at $\delta = +0.4$

The resulting heat diffusivity profiles are plotted in figure 10. It appears clearly that for large radii, $\rho > 0.45$, the variation of χ_e with plasma shape is not due to the small variations of Q_e, n_e, $< |\nabla\rho|^2 >$: in this region, profile 2 is similar to profile 1, and profile 3 is similar to profile 4. For $0.25 < \rho < 0.45$, the higher heat diffusivity observed at $\delta = +0.4$ compared to $\delta = -0.4$ is due to a slightly more central EC power deposition, leading to a higher heat flux in this region, which tends to decrease the temperature variation with triangularity for $\rho < 0.45$. To sum up, the reduction of electron heat transport, observed when decreasing the plasma triangularity from $\delta = +0.4$ to $\delta = -0.4$ is not due to a variation of the flux surfaces compression, Q_e or n_e, but should be attributed to the variation of plasma triangularity. This reduction of electron heat transport with plasma triangularity is significant. Reducing the triangularity from $\delta = +0.4$ to $\delta = -0.4$, the electron energy confinement time $\tau_E e$ increases from 3.6 to 5.3 ms and the electron energy confinement time normalized to the RLW model prediction [] increases from 1.5 to 2.2. As a consequence, to obtain the

same temperature profile, only half of the EC power used at $\delta = +0.4$ ($P_{EC} = 1.3\,\mathrm{MW}$) is required at $\delta = -0.4$ ($P_{EC} = 0.6\,\mathrm{MW}$), keeping constant the line averaged density and edge safety factor, see figure 11.

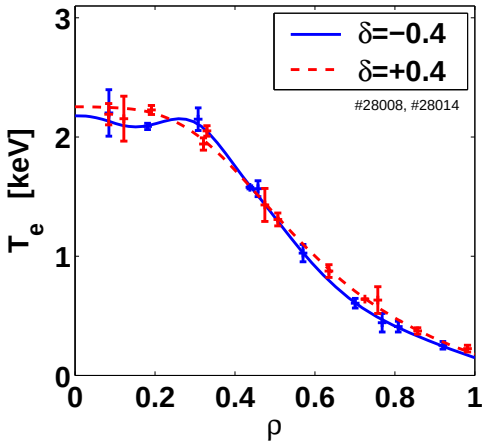

Figure 11. The same T_e profile is obtained at $\delta = -0.4$ (——) as compared to $\delta = +0.4$ (– – –) with half less EC power (0.6 MW instead of 1.3 MW). The line averaged density and edge safety factor are kept constant.

5.2. Plasma shape variation in LORB5

To test the possible influence of plasma shape on ITG/TE modes stability, we performed simulations with the global linear collisionless gyro-kinetic code LORB5 [23]. The code LORB5 is coupled with the CHEASE code, a Grad-Shafranov solver of tokamak plasmas MHD-equilibria [29]. The T_e, T_i and n_e profiles used in the simulation are the ones taken from the experimental $\delta = 0.2$ equilibrium indicated in figure 4. The triangularity of the last closed flux surface is varied from -0.3 to 0.5 and the corresponding plasma equilibrium is reconstructed using CHEASE. As mentioned in section 3, the dominant instability in these conditions is a TE mode. The global mode growth rate and average radial extension does not depend significantly on the plasma triangularity, figure 12a, but the radial localization and structure of the electrostatic potential fluctuations, $\tilde{\Phi}$, changes with δ, being displaced inwards toward negative triangularities, figure 12a. The change of the $\tilde{\Phi}$ localization and structure with δ can not easily be translated in terms of electron heat transport but underlines, together with the experimental observation of an increase of electron heat transport with δ, that the full plasma geometry should be taken into account in the simulation of ITG-TE modes.

6. Collisionality effect

In TCV, the electron heat transport is observed to strongly decrease with increasing collisionality for all the range of plasma triangularities explored, figure 13a and b. In

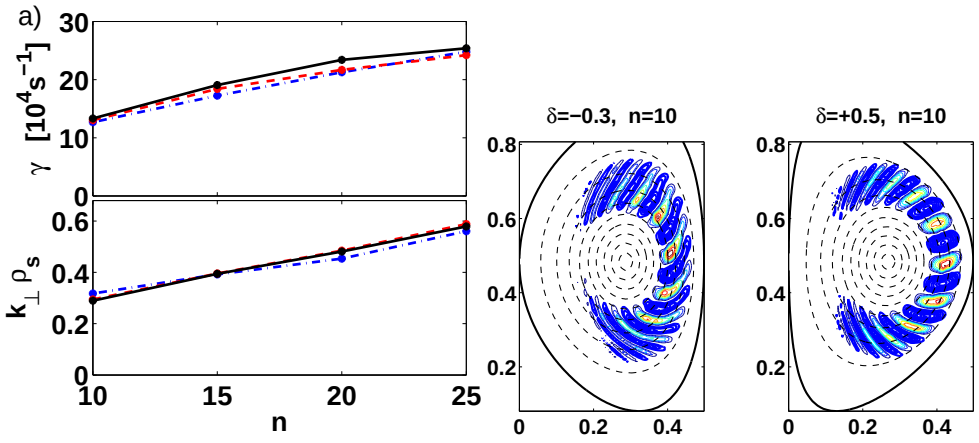

Figure 12. a) LORB5 simulations showing the variation of the mode growth rate with the plasma triangularity for toroidal mode numbers ranging from 10 to 25
b) Poloidal structure of the electrostatic potential at $\delta = -0.3$ and $\delta = +0.5$, for toroidal mode number $n = 10$.

figure 13a, the electron heat diffusivity calculated at $\rho = 0.53$, between the two EC power deposition radii, is plotted as a function of the effective collisionality $\nu_{\rm eff}$ for both triangularities, $\delta = 0.2$ and $\delta = 0.4$, of the "constant $I_{\rm p}$" set of experiments. The electron heat diffusivity $\chi_{\rm e}$ decreases with increasing $\nu_{\rm eff}$ and no dependence on the plasma triangularity is observed. In this set of experiments, the value of $n_{\rm e}Z_{\rm eff}$ at mid-radius is significantly higher at $\delta = 0.2$ compared to $\delta = 0.4$ and figure 13a suggests strongly that the $\chi_{\rm e}$ dependence on $T_{\rm e}$ discussed in section 4.1, observed at $\delta = 0.4$ at constant $n_{\rm e}Z_{\rm eff}$, is a dependence on $\nu_{\rm eff}$. It is however not excluded that $\chi_{\rm e}$ could depend on both $\nu_{\rm eff}$ and $T_{\rm e}$ independently. The observation of a reduction of $\chi_{\rm e}$ with increasing $\nu_{\rm eff}$ in TCV is consistent with the expected stabilization of TE modes at high collisionality, shown in GLF23 simulations, and with the reduction of electron heat transport with increasing $\nu_{\rm eff}$ observed in ASDEX Upgrade L-mode plasmas []. In figure 13b, $\chi_{\rm e}$ is plotted as a function of the effective collisionality for the "constant q_{95}" set of experiments. Here also, $\chi_{\rm e}$ is observed to decrease with increasing $\nu_{\rm eff}$ and does not depend significantly on triangularity for positive δ values. However, at negative triangularity, $\chi_{\rm e}$ decreases with decreasing δ, as was observed in section 5.1. The coupled effect of $\nu_{\rm eff}$ and δ allows us to understand why the reduction of electron heat transport observed when reducing δ from $+0.4$ to -0.4 is modest at constant heat flux, while it has a strong impact on the required amount of EC power to achieve a given temperature. At constant heat flux and plasma density, the reduction of $\chi_{\rm e}$ with decreasing δ leads to an increase of $T_{\rm e}$, and therefore to $1/\nu_{\rm eff}$, which in turn lead to an increase of $\chi_{\rm e}$ and limit the increase of $T_{\rm e}$. The strong reduction of $\chi_{\rm e}$ with δ is masked by the increase an increase of $1/\nu_{\rm eff}$. On the other hand, if the effective collisionality is kept constant by adjusting the heat flux, the strong reduction of $\chi_{\rm e}$ with δ appears clearly in the reduction of the EC power required to obtain the same electron temperature at $\delta = -0.4$ than at

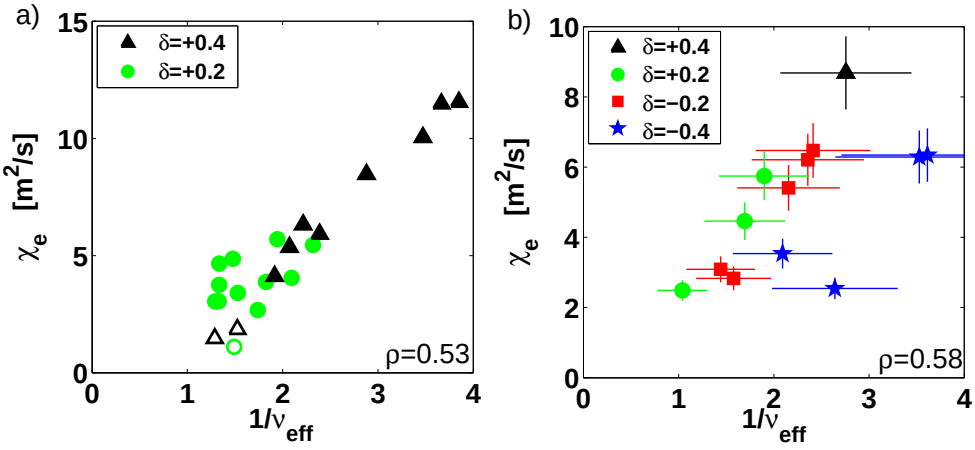

Figure 13. Electron heat transport reduction at high plasma collisionality in (a) the "constant I_p" (open symbols indicates point where ITG dominates according to GLF23 simulations) and (b) the "constant q_{95}" set of experiments. In the "constant q_{95}" set of experiments, a large range of plasma triangularity is explored and electron heat transport is observed to reduce at negative triangularity.

$\delta = +0.4$.

To check that the variation of χ_e with ν_{eff} is not only due to a $T_e^{3/2}$ gyro-Bohm dependence, we plot χ_e/f_{GB} as a function of $1/\nu_{eff}$ in figure 14. It appears that an increase of the plasma collisionality and a decrease of the plasma triangularity still leads to a reduction of electron heat transport, even with a gyro-Bohm normalization. The χ_e dependence on T_e of the gyro-Bohm scaling could be correct, but has to be completed with a ν_{eff} and a δ dependence.

7. Conclusion

Electron heat transport in low density L-mode plasmas has been investigated in TCV using strong localized EC heating. In these experimental conditions, both local linear gyro-fluid simulations (GLF23) and global collisionless gyro-kinetic simulations (LORB5) indicate that TE modes should play a crucial role in the transport of electron heat. In the simulations, the TE modes growth rate is found to strongly depend on the electron temperature T_e and on the normalized temperature gradient R/L_{T_e}. The electron heat transport dependence on these two parameters has therefore been tested experimentally by varying independently T_e and R/L_{T_e} over a large, earlier unexplored range. The electron temperature was changed mainly by changing the amount of EC power deposited in the discharge, while the temperature gradient was changed by changing the radial EC power distribution. The electron heat diffusivity, calculated at mid-radius, is found to strongly increase with the electron temperature with no strong dependence on R/L_{T_e} nor R/L_{n_e}, except at the lowest R/L_{T_e} values if a gyro-Bohm dependence is assumed for χ_e. This result has been obtained at constant $n_e Z_{eff}$.

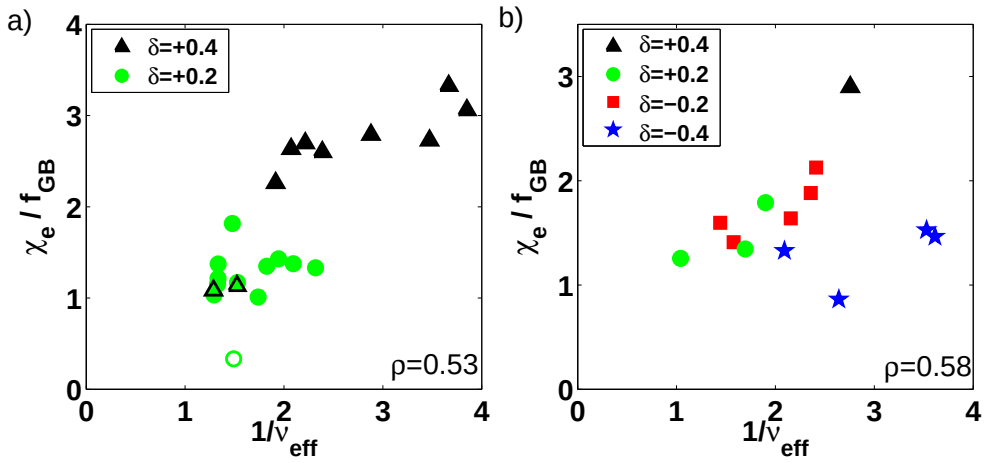

Figure 14. Electron heat diffusivity normalized to gyro-Bohm scaling as a function of plasma collisionality in (a) the "constant I_p" (open symbols indicates point where ITG dominates according to GLF23 simulations) and (b) the "constant q_{95}" set of experiments. In the "constant q_{95}" set of experiments, a large range of plasma triangularity is explored and electron heat transport is observed to reduce at negative triangularity.

Comparing data with different values of $n_e Z_{eff}$, it appears first that χ_e depends on T_e but also on $n_e Z_{eff}$ and second that the electron heat diffusivity, as well as the electron heat diffusivity normalized a gyro-Bohm scaling, are shown to reduce strongly with increasing effective collisionality $\nu_{eff} = 0.1R\frac{n_e Z_{eff}}{T_e^2}$. This reduction of electron heat transport with ν_{eff} is consistent with the strong experimental impact of the effective collisionality on particle transport and with the predicted stabilizing effect of ν_{eff} on the TE modes. It is however not excluded that χ_e could depend independently on T_e and ν_{eff}. These results suggest that the effective collisionality has to be included in the heuristic modelling of electron heat transport, together with a decrease of the impact of R/L_{T_e} on χ_e at high R/L_{T_e} values. In future reactor level experiments, like ITER, due to the strong electron heating by alpha particles, a low collisionality is expected and the observed dependence of electron heat transport on ν_{eff} could play a significant role. In addition, the TCV plasma shaping capabilities have been exploited to test the influence of plasma triangularity on electron heat transport. It appears that electron heat transport decreases with decreasing triangularity. The effect is relatively weak from $\delta = +0.4$ to $\delta = -0.2$ but becomes much more pronounced at $\delta = -0.4$. At constant collisionality, half less EC power is required at $\delta = -0.4$ as compared to $\delta = +0.4$ to obtain the same electron temperature.

Acknowledgments

The authors would like to acknowledge fruitful discussions with C. Angioni and L. Villard.

Global simulations were performed on the parallel servers SGI Origin 3800 and the Linux cluster PLEIADES of the Ecole Polytechnique Fédérale de Lausanne.

References

[1] F. Troyon, R. Gruber, H. Saurenmann, S. Semenzato, and S. Succi. *Plasma Phys. Control. Fusion*, 26:209, 1984.
[2] F. Hofmann, O. Sauter, H. Reimerdes, I. Furno, and A. Pochelon. *Phys. Rev. Lett.*, 81:2918, 1998.
[3] M. Greenwald, J.L. Terry, S.M. Wolfe, S. Ejima, M.G. Bell, S.M. Kaye, and G.H. Neilson. *Nucl. Fusion*, 28:2199, 1988.
[4] H. Reimerdes, A. Pochelon, O. Sauter, T.P. Goodman, M.A. Henderson, and An. Martynov. *Plasma Phys. Control. Fusion*, 42:629, 2000.
[5] J. Stober, O. Gruber, A. Kallenbach, V. Mertens, F. Ryter, A. Stabler, W. Suttrop, W. Treutterer, and the ASDEX Upgrade Team. *Plasma Phys. Control. Fusion*, 42, 2000.
[6] G. Saibene, R. Sartori, A. Loarte, D.J. Campbell, P.J. Lomas, V. Parail, K.D. Zastrow, Y. Andrew, S. Sharapov, A. Korotkov, M. Becoulet, G.T.A. Huysmans, H.R. Koslowski, R. Budny, G.D. Conway, J. Stober, W. Suttrop, A. Kallenbach, M. von Hellermann, and M. Beurskens. *Plasma Phys. Control. Fusion*, 44:1769, 2002.
[7] J.-M. Moret, S. Franke, H. Weisen, M. Anton, R. Behn, B.P. Duval, F. Hofmann, B. Joye, Y. Martin, C. Nieswand, Z.A. Pietrzyk, and W. van Toledo. *Phys. Rev. Lett.*, 79:2057, 1997.
[8] H. Weisen, J.-M. Moret, S. Franke, I. Furno, Y. Martin, M. Anton, R. Behn, M.J. Dutch, B.P. Duval, F. Hofmann, B. Joye, C. Nieswand, Z.A. Pietrzyk, and W. Van Toledo. *Nucl. Fusion*, 37:1741, 1997.
[9] F. Hofmann et al. *Plasma Phys. Control. Fusion*, 43, 2001.
[10] A. Pochelon, T.P. Goodman, and M.A. Henderson et al. *Nucl. Fusion*, 39:1807, 1999.
[11] A. Pochelon et al. *Proc. 26th EPS Conference on Controlled Fusion and Plasma Physics (Maastricht, Netherlands)*, 23J:1089, 1999.
[12] C. Angioni, A.G. Peeters, G.V. Pereverzev, F. Ryter, and G. Tardini. *Phys. Rev. Lett.*, 90:205003, 2003.
[13] H. Weisen, A. Zabolotsky, C. Angioni, I. Furno, X. Garbet, C. Giroud, H. Leggate, P. Mantica, D. Mazon, J. Weiland, L. Zabeo, and K.-D. Zastrow. *Nucl. Fus.*, 45, 2005.
[14] C. Angioni, A.G. Peeters, X. Garbet, A. Manini, and F. Ryter. *Nucl. Fus.*, 44:827, 2004.
[15] T.P. Goodman, S. Alberti, M.A. Henderson, A. Pochelon, and M.Q. Tran. *Proc. 19th Symposium on Fusion Technology (Lisbon, Portugal)*, I:565, 1996.
[16] J.-P. Hogge, S. Alberti, L. Porte, and G. Arnoux. *Nucl. Fusion*, 43:1353, 2003.
[17] C. Angioni, T.P. Goodman, M.A. Henderson, and O. Sauter. *Nucl. Fus.*, 43:455, 2003.
[18] K. Matsuda. *IEEE Trans. Plasma Sci.*, 17:6, 1989.
[19] F. Ryter, C. Angioni, M. Beurskens, S. Cirant, G.T. Hoang, G.M.D. Hogeweij, F. Imbeaux, A. Jacchia, P. Mantica, W. Suttrop, and G. Tardini. *Plasma Phys. Control. Fusion*, 43:A323, 2001.
[20] F. Ryter, G. Tardini, F. De Luca, H.-U. Fahrbach, F. Imbeaux, A. Jacchia, K.K. Kirov, F. Leuterer, P. Mantica, A.G. Peeters, G. Pereverzev, and W. Suttrop. *Nucl. Fus.*, 43:1396, 2003.
[21] F. Jenko, W. Dorland, and G.W. Hammett. *Phys. Plasmas*, 8:4096, 2001.
[22] W. Dorland G. W. Hammett M. Kotschenreuther R. E. Waltz, G. M. Staebler and J. A. Konings. *Phys. Plasmas*, 4:2482, 1997.
[23] A. Bottino, A.G. Peeters, O. Sauter, J. Vaclavik, and L. Villard. *Phys. Plasmas*, 11:198, 2004.
[24] C. Angioni, A.G. Peeters, G.V. Pereverzev, F. Ryter, and G. Tardini. *Phys. Plasmas*, 10:3225, 2003.
[25] Y.R. Lin-Liu and R.L. Miller. *Phys. Plasmas*, 2:1666, 1995.
[26] S. Cirant, S. Alberti, F. Gandini, R. Behn, T.P. Goodman, and P. Nikkola. *Nucl. Fus.*
[27] F. Imbeaux, F. Ryter, and X. Garbet. *Plasma Phys. Control. Fusion*, 43:1503, 2001.

[28] X. Garbet, P. Mantica, F. Ryter, G. Cordey, F. Imbeaux, C. Sozzi, A. Manini, E. Asp, V. Parail, and R. Wolf. *Plasma Phys. Control. Fusion*, 46:1351, 2004.
[29] H. Lütjens, A. Bondeson, and A. Roy. *Conput. Phys. Comm.*, 69:287, 1992.